doi:10.3788/gzxb20144306.0630003

基于同心离轴双反射系统成像光谱仪的像散校正

陈廷爱,唐义,张丽君,常月娥,郑成

(北京理工大学 光电学院 光电成像技术与系统教育部重点实验室,北京 100081)

摘 要:提出了一种基于同心离轴双反射系统的成像光谱仪,该系统由四片球面反射镜与一块平面光栅组成.在分析同心离轴双反射系统的基础上,结合像差理论与光程函数概念,推导了同心离轴双反射系统的像散公式,得到其消像散条件.消像散理论表明,将消像散的同心离轴双反射系统分别应用于成像光谱仪的准直光路与聚焦光路中,可以实现成像光谱仪全光路消像散.研究了准直光路与聚焦光路共心对称的成像光谱仪结构,给出了其通用设计算法.根据初始结构计算方法,设计了工作波段在远紫外(120~180 nm)的成像光谱仪实例,给出了初始结构的点略图与像散曲线图,以验证消像散理论的正确性.结果表明,初始结构完全符合消像散理论.优化设计后的成像光谱仪光谱分辨率接近 1.6 nm,调制传递函数值全视场全波段在 0.37 以上,具有良好的成像质量.

关键词:成像光谱仪;像散;光程;同心离轴双反射系统;光学设计

中图分类号:O433.1; TH744.1 **文献标识码**:A **文章编号**:1004-4213(2014)06-0630003-8

Astigmatism Compensation in Imaging Spectrometer Based on Concentric Off-axis Dual Reflector System

CHEN Ting-ai, TANG Yi, ZHANG Li-jun, CHANG Yue-e, ZHENG Cheng

(*Key Laboratory of Photoelectronic Imaging Technology and System, Ministry of Education of China School of Optoelectronics, Beijing Institute of Technology, Beijing* 100081, *China*)

Abstract: A specific imaging spectrometer based on concentric off-axis dual reflector system was proposed which consisted of four spherical mirrors and a plane grating. On the basis of analysis of the concentric off-axis dual reflector system, aberration theory and optical path-length concept were used to derive an expression for the separation of astigmatic images in concentric off-axis dual reflector system, the astigmatism elimination in which was found further. It is shown that the astigmatism of the imaging spectrometer can be eliminated by applying concentric off-axis dual reflector system without astigmatism in both the collimating and condensing optics. A symmetrical and concentric imaging spectrometer was described and a generalized design procedure was shown. The symmetrical and concentric imaging spectrometer working in far-ultraviolet (120~180 nm) wavelength was simulated by applying the design procedure. To verify the stigmatic principle, spot diagram and the curves of astigmatism were shown. The results show that the initial structure satisfies the stigmatic principle well. The spectral resolution of the optimized spectrometer is close to 1.6 nm and the modulation transfer function is more than 0.37 for the total field of view at all wavelengths, which provides good imaging quality.

Key words: Imaging spectrometer; Astigmatism; Optical path-length; Concentric off-axis dual

Foundation item: The National Key Basic R&D Program of China (No. 2013CB329202) and the Basic Industrial Technology Project (No. J312012B002)

First author: CHEN Ting-ai(1988-), male, M. S. degree candidate, mainly focuses on optical design, optical alignment and radiance calibration of ultraviolet imaging spectrometer. Email:cntgai@163.com

Supervisor(Contact author): TANG Yi(1977-), male, associate professor, Ph. D. degree, mainly focuses on UV communication and ultraviolet imaging spectral technique. Email:tangyi4510@bit.edu.cn

Received: Oct. 8, 2013; **Accepted**: Dec. 18, 2013

reflector system; Optical design
OCIS Codes: 300.6190; 220.1000; 120.4570; 120.6200

0 Introduction

Imaging spectrometer is designed to measure one-dimensional spectral information and two-dimensional spatial information in image position[1]. The far-ultraviolet imaging spectrometer is one of the most frequently used instruments for detecting atmosphere and ionosphere, where high spatial resolution to observe target properties and high spectral resolution to separate adjacent spectral lines need to be provided simultaneously. At present, different structured spectrometers carried by satellite can′t achieve satisfactory imaging quality. Higher imaging quality demands that the optical structure carries on advanced processing, like toroidal grating used in GUVI[2]. It is necessary to propose a new imaging spectrometer to improve the shortcomings.

In a conventional Czerny-Turner spectrometer with a plane grating and two spherical mirrors, the mount can be configured to correct coma aberration[3-4], but astigmatism yielding different focal lengths in the sagittal and tangential planes due to off-axis incidence on mirrors remains in the configuration. It can be ignored in spectrometer with single-channel detector, because the longitudinal size of the detector is much larger than the elongated slit image along the slit-height (sagittal) direction. However, the existence of astigmatism will deteriorate the image quality in spectrometers using multichannel detector[5]. In this respect, a variety of methods have been proposed to reduce or remove the astigmatism. Such as: using free-form mirrors[6] or toroidal mirrors[7] instead of the spherical condensing mirrors, or replacing the plane grating with cylindrical grating[8], the disadvantage of these methods is that they increase the cost and the difficulty of processing due to the use of aspherical mirrors or aplanar gratings. The use of the grating in divergent illumination is introduced to eliminate astigmatism[9], but the divergent illumination approach will limit the F number of the optics and deteriorate the image quality. Placing a cylindrical lens after the focusing mirror[10], it is a pity that the glass for some optical transmission spectra (like far-ultraviolet band) is rare; the proposal to add extra convex mirrors for astigmatism elimination in concave mirrors[11], but the author did not study specific designs. Adding compensating optics before the entrance slit[12], which makes the structure of optics more complicated.

Although the Czerny-Turner spectrometer is an appropriate instrument for those experiments which need high spectral resolution, its stigmatic structure can′t provide a good spatial resolution. So it is rarely used as imaging spectrometer for remote sensing. A special system named schwarzschild imaging spectrometer was introduced and analyzed by author Mouriz[13]. A condition for elimination of astigmatism according to ray tracing and analytic theory was presented in that paper. Differently, here another form of the astigmatism elimination condition based on aberration theory and optical path-length concept was found and derived, which has been proven identical to the equation derived.

Before we go any further to study the spectrometer, astigmatism in the concentric off-axis dual reflector system should be analyzed. It means that if an astigmatism elimination condition can be established, a specific concentric and symmetrical spectrometer based on concentric off-axis dual reflector system will be designed. A general theory of aberrations for the off-axis spherical mirror is derived firstly based on the optical path-length concept. Subsequently, the separation of astigmatic images in concentric off-axis dual reflector system is given and condition for astigmatic elimination is derived. Then we describe the spectrometer and show a generalized design procedure. To verify the sigmatic principle, a far-ultraviolet spectrometer example with excellent performance is presented.

1 Concentric off-axis dual reflector system

The proposal of this paper is a distinctive spectrometer (hereafter, the spectrometer in the following paper represents the imaging spectrometer), in which both the collimating and the condensing optics are concentric off-axis dual reflector system. As can be seen from Fig. 1, the system consists of one plane grating and four spherical mirrors. In addition, by making

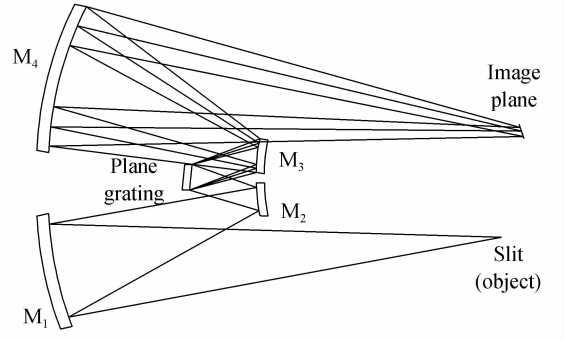

Fig. 1 Schematic of optical path for spectrometer based on concentric off-axis dual reflector system

convex mirrors and concave mirrors have the same radius of curvature respectively ($R_2 = R_3$, $R_1 = R_4$), a symmetrical and concentric configuration can be achieved.

Fig. 2 shows the configuration of the concentric off-axis dual reflector system with off-axis illumination. A parallel bundle of rays coming from the

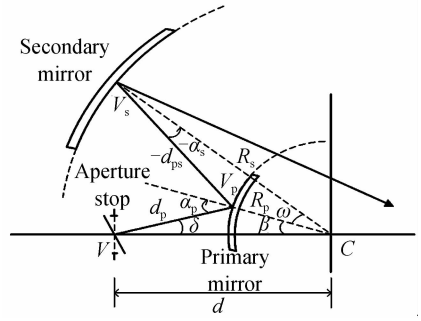

Fig. 2 Concentric off-axis dual reflector system; primary mirror is convex; secondary mirror is concave; aperture stop at the grating position in spectrometer is displaced from the first mirror

aperture stop first falls on the convex mirror and is reflected to the concave mirror, which brings the rays into focus. Applying the sine theorem to $\Delta V_s V_p C$ and $\Delta V V_p C$ mathematically

$$\frac{R_p}{\sin\alpha_s}=\frac{d_{ps}}{\sin\omega}=\frac{R_s}{-\sin\alpha_p} \tag{1}$$

$$\alpha_p=-\alpha_s+\omega \tag{2}$$

$$\frac{R_p}{\sin\delta}=\frac{d_p}{\sin\beta}=\frac{d}{\sin\alpha_p} \tag{3}$$

$$\alpha_p=\beta+\delta \tag{4}$$

R_p and R_s are the radius of primary mirror and secondary mirror respectively, they are positive if the direction from vertex to the center of curvature is coincident with that of the light; d_{ps} is the distance between the primary mirror and the secondary mirror, measured along the chief ray. d_{ps} becomes positive when the primary mirror is located to the left of the secondary mirror; the incidence angles of chief ray at the primary mirror and secondary mirror are given by α_p and α_s respectively, they are positive for clockwise rotation of the light; the angle w is measured from the primary mirror normal to the secondary mirror normal, it is positive if the rotation is in the clockwise direction. d is the distance between the common center of two mirrors and the center of aperture stop.

2 Optical path length

In order to deal with the off-axis systems, the local coordinate is used to replace the global coordinate. According to coordinate transformation theory, the surface function of sphere keeps unchanged from global coordinate to local coordinate and it can be represented by

$$x'^2+y'^2-2Rz'+z'^2=0 \tag{5}$$

To obtain a form suitable to calculate the optical path length, which needs powers of x and y, Eq. (5) is expanded in a power series of x and y

$$z=R-\left[R^2-(x^2+y^2)\right]^{+}\approx\frac{x^2+y^2}{2R}+\frac{(x^2+y^2)^2}{8R^3}+\frac{(x^2+y^2)^3}{16R^5}+\cdots \tag{6}$$

As the image quality criteria, wave-front and ray aberrations can be obtained from the optical path length between the object and the image[14-15]. In Fig. 3, both the object distance r and the image distance r' are measured along the chief ray; the incidence angle α are

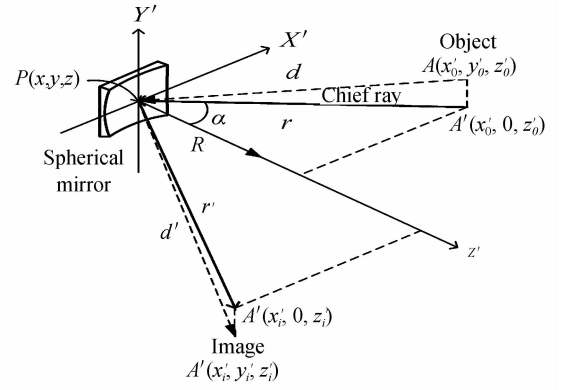

Fig. 3 Optical path length by the spherical mirror

positive for clockwise rotation of the light. Light coming from the object point $A(x'_0, y'_0, z'_0)$ falls on an arbitrary point $P(x, y, z)$ of the spherical mirror (which is the origin of the converted coordinate) and is reflected to the image point $A'(x'_i, y'_i, z'_i)$. The corresponding optical path length is given as

$$OPL=A'P+AP \tag{7}$$

$$AP^2=(x-x'_0)^2+(y-y'_0)^2+(z-z'_0)^2 \tag{8}$$

$$A'P^2=(x-x'_i)^2+(y-y'_i)^2+(z-z'_i)^2 \tag{9}$$

To simplify the calculation, from now on only objects and images lying on the $y'=0$ plane are considered. Despite the loss of generality, there exists essential information in the formulation to obtain significant results[15]. According to the geometric relationships in Fig. 3, the image and object coordinates are introduced as follows

$$x'_0=r\sin\alpha \tag{10}$$

$$z'_0=r\cos\alpha \tag{11}$$

$$x'_i=-r'\sin\alpha \tag{12}$$

$$z'_i=r'\cos\alpha \tag{13}$$

Substituting Eqs. (6), (10), (11), (12), (13) in Eq. (8) yields

$$AP^2=\left(1-\frac{r}{R}\cos\alpha\right)\left[x^2+y^2+\frac{(x^2+y^2)^2}{4R^2}+\frac{(x^2+y^2)^3}{8R^4}+\cdots\right]+r^2-2xr\sin\alpha=r^2-2xr\sin\alpha+x^2\sin^2\alpha+x^2\cos^2\alpha-x^2\frac{r}{R}\cos\alpha+\left(1-\frac{r}{R}\cos\alpha\right)y^2+\left(1-\frac{r}{R}\cos\alpha\right)\left[\frac{(x^2+y^2)^2}{4R^2}+\frac{(x^2+y^2)^3}{8R^4}+\cdots\right] \tag{14}$$

The square root can be expanded using power series expansion with respect to $r-x\sin\alpha$ to obtain

$$AP=(r-x\sin\alpha)\left\{1+\frac{1}{2}\left[x^2\frac{\cos^2\alpha-\frac{r}{R}\cos\alpha}{(r-x\sin\alpha)^2}+y^2\frac{1-\frac{r}{R}\cos\alpha}{(r-x\sin\alpha)^2}+\frac{(x^2+y^2)^2}{4R^2}\frac{1-\frac{r}{R}\cos\alpha}{(r-x\sin\alpha)^2}+\frac{(x^2+y^2)^3}{8R^4}\frac{1-\frac{r}{R}\cos\alpha}{(r-x\sin\alpha)^2}+\cdots\right]\right\} \tag{15}$$

Substituting the power series expansion of $\frac{1}{r-x\sin\alpha}$ into Eq. (15) yeilds

$$\begin{aligned}AP=&r-x\sin\alpha+\frac{x^2}{2}\left(\frac{\cos^2\alpha}{r}-\frac{\cos\alpha}{R}\right)+\frac{y^2}{2}\left(\frac{1}{r}-\frac{\cos\alpha}{R}\right)+\frac{(x^2+y^2)^2}{8R^2}\left(\frac{1}{r}-\frac{\cos\alpha}{R}\right)+\frac{(x^2+y^2)^3}{16R^4}\left(\frac{1}{r}-\frac{\cos\alpha}{R}\right)+\\&\cdots+\frac{1}{2}x^3\frac{\sin\alpha}{r}\left(\frac{\cos\alpha^2}{r}-\frac{\cos\alpha}{R}\right)+\frac{1}{2}y^2\frac{x\sin\alpha}{r}\left(\frac{1}{r}-\frac{\cos\alpha}{R}\right)+\frac{(x^2+y^2)^2}{8R^2}\frac{x\sin\alpha}{r}\left(\frac{1}{r}-\frac{\cos\alpha}{R}\right)+\\&\frac{(x^2+y^2)^3}{16R^4}\frac{x\sin\alpha}{r}\left(\frac{1}{r}-\frac{\cos\alpha}{R}\right)+\cdots+\frac{1}{2}\frac{x^4}{r^2}\sin^2\alpha\left(\frac{\cos^2\alpha}{r}-\frac{\cos\alpha}{R}\right)+\frac{1}{2}y^2\frac{x^2}{r^2}\sin^2\alpha\left(\frac{1}{r}-\frac{\cos\alpha}{R}\right)+\\&\frac{(x^2+y^2)^2}{8R^2}\frac{x^2\sin^2\alpha}{r^2}\left(\frac{1}{r}-\frac{\cos\alpha}{R}\right)+\cdots\end{aligned} \tag{16}$$

$A'P$ can be approximated similarly, Substituting Eq. (16) and the similar expansion of $A'P$ in Eq. (7) finally yields

$$OPL=AP+A'P=r+r'+A_1x^2+A_1'y^2+A_2x^3+A_2'xy^2 \tag{17}$$

$$A_1=\frac{1}{2}\left(\frac{\cos^2\alpha}{r}+\frac{\cos^2\alpha}{r'}-\frac{2\cos\alpha}{R}\right) \tag{18}$$

$$A_1'=\frac{1}{2}\left(\frac{1}{r}+\frac{1}{r'}-\frac{2\cos\alpha}{R}\right) \tag{19}$$

$$A_2=\frac{1}{2}\left[\frac{\sin\alpha}{r}\left(\frac{\cos^2\alpha}{r}-\frac{\cos\alpha}{R}\right)-\frac{\sin\alpha}{r'}\left(\frac{\cos^2\alpha}{r'}-\frac{\cos\alpha}{R}\right)\right] \tag{20}$$

$$A_2'=\frac{1}{2}\left[\frac{\sin\alpha}{r}\left(\frac{1}{r}-\frac{\cos\alpha}{R}\right)-\frac{\sin\alpha}{r'}\left(\frac{1}{r'}-\frac{\cos\alpha}{R}\right)\right] \tag{21}$$

The second-order terms A_1x^2 and $A_1'y^2$ in Eq. (17) represent astigmatism, the coefficients A_1 and A_1' gives the tangential and sagittal astigmatic image locations respectively. The third-order terms A_2x^3 and $A_2'xy^2$ in Eq. (17) are associated with coma. Note that astigmatism is the lowest-order aberration present in single off-axis spherical mirror and is mostly responsible for the image degradation. So the astigmatism which is the major aberration of concentric off-axis dual reflector system will be studied in the following work. As for coma, it loses relevance to study in concentric off-axis dual reflector system unless astigmatism is eliminated. Actually, in the following practical design and simulation, the residual coma has a quite small value (In the initial configuration with central wavelength $\lambda_0=150$ nm, the magnitude of the coma coefficient W_{131} is about $0.3\ \lambda_0$).

3 Astigmatism calculation of concentric off-axis dual reflector system

The second-order terms A_1x^2 and $A_1'y^2$ in Eq. (17) is zero if $A_1=0$ and $A_1'=0$, then the locations of tangential and sagittal astigmatic image with corresponding object locations r_t and r_s can be yielded

$$\frac{1}{r_t'}=\frac{2}{R\cos\alpha}-\frac{1}{r_t} \tag{22}$$

$$\frac{1}{r_s'}=\frac{2\cos\alpha}{R}-\frac{1}{r_s} \tag{23}$$

Eqs. (22) and (23) represent the off-axis astigmatism which has the same form as on-axis astigmatism. With regard to the concentric off-axis dual reflector system, the object locations of the secondary mirror r_{2-t} and r_{2-s} both measured along the chief ray can be expressed as

$$r_{2-t}=r_{1-t}'-d_{ps} \tag{24}$$

$$r_{2-s}=r_{1-s}'-d_{ps} \tag{25}$$

Since the first mirror is illuminated in collimated light, substitution of $r_{1-s}=r_{1-t}=\infty$ in Eqs. (22), (23) yields the tangential and sagittal image locations of the primary mirror r_{1-t}' and r_{1-s}'. Substituting them in Eqs. (24), (25) and using Eqs. (22), (23) at the secondary mirror again, the tangential and sagittal image locations of the secondary mirror can be respectively expressed as

$$r_{2-t}'=-\frac{R_p\sin\alpha_p\cos\alpha_s(\sin\omega+\sin\alpha_p\cos\alpha_s)}{2\sin\omega\sin\alpha_s} \tag{26}$$

$$r_{2-s}'=\frac{R_p\sin\alpha_p(\sin\alpha_s-2\cos\alpha_p\sin\omega)}{2\sin\omega\sin\alpha_s\cos\omega} \tag{27}$$

The astigmatic images' separation Δr of the concentric off-axis dual reflector system is obtained as

$$\Delta r=r_{2-s}'-r_{2-t}'=R_p\sin\alpha_p\left[-\frac{\tan\omega}{2}-\left(\frac{2}{\tan\alpha_p}+\frac{2}{\tan\alpha_s}\right)\right]^{-1} \tag{28}$$

The astigmatism of the concentric off-axis dual reflector system can be corrected by imposing the condition

$$\frac{1}{\tan\alpha_p}+\frac{1}{\tan\alpha_s}+\frac{1}{\tan\omega}=0 \tag{29}$$

This is the most important condition for the concentric off-axis dual reflector system since it makes the performance of them comparable to on-axis systems. In fact, Eq. (29) can be transformed into another form

$$\tan 2\omega=2(\tan\alpha_p+\tan\alpha_s) \tag{30}$$

which is the stigmatic condition given by author Mouriz. Combining Eqs. (2) and (29), the angle w can be derived as a function of α_p

$$\tan\omega=\frac{\tan\alpha_p}{2}\frac{-1+\sqrt{5+4\tan\alpha_p^2}}{1+\tan\alpha_p^2} \tag{31}$$

In order to design a concentric off-axis dual reflector system, several possible combinations of parameters, like α_p and R_p (α_s and R_s) are chosen before the computation. Then the remaining parameters that define the system can be calculated by applying the formulas of section 1 to receive a stigmatic instrument.

4 Spectrometer based on concentric off-axis dual reflector system

The structural schematic of spectrometer based on concentric off-axis dual reflector system is shown in Fig. 4, the common center of curvature of the four mirrors is located at C, the grating center is located at V. The slit and the grating rulings are orthogonal to the meridional plane (the plane of drawing), and it is assumed that the grating acts as the aperture stop. The ray path $V_1V_2VV_3V_4$ passing through the center of slit is the chief ray for an arbitrary wavelength. The collimated beam produced by the first two mirrors is incident on the grating in a direction which makes an angle δ with VC , and the diffracted beam makes an angle δ' with VC. To guarantee the symmetrical and concentric configuration and to eliminate astigmatism simultaneously, a condition should be met

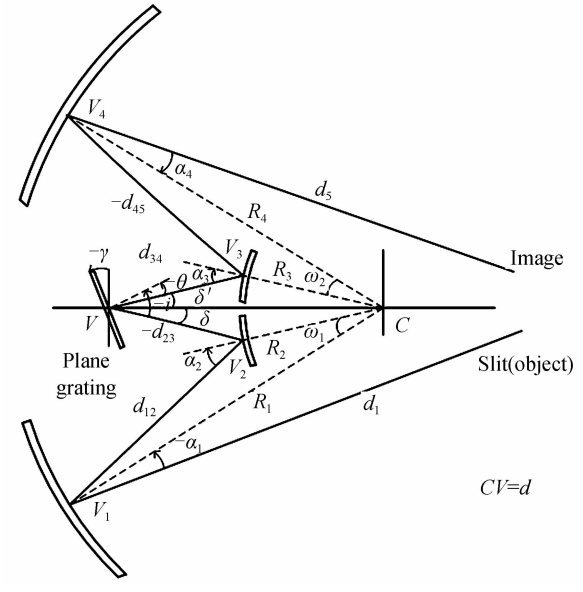

Fig. 4 Structural schematic of spectrometer based on concentric off-axis dual reflector system

$$\delta=\delta' \tag{32}$$

and the diffraction grating should be rotated an suitable angle γ with respect to VC's perpendicular. The angle γ is positive when the grating lies in a clockwise direction with respect to VC's perpendicular. Then the relationship between the incidence angle i (the diffraction angle θ) and angle δ (δ') in Fig. 4 is

$$-i=-\gamma+\delta \tag{33}$$

$$-\theta=-\gamma-\delta' \tag{34}$$

$$\sin(\gamma-\delta)+\sin(\gamma+\delta')=mg\lambda \tag{35}$$

where m is the diffraction order and g is the groove density.

In the calculation of spectrometer parameters, the incidence angle i and diffraction angle θ are uniquely determined by the following equation, if the wavelength λ and the rotation angle of grating γ is given as

$$2\sin\gamma\cos\delta=mg\lambda \tag{36}$$

To verify the developed theory, a spectrometer based on concentric off-axis dual reflector system is designed and analyzed. Before doing so, a design procedure based on the previous works is introduced. The design procedure starts by choosing the groove density g, the grating order m, the design wavelength λ, the rotation angle of grating γ, the convex mirror radius R_p, the convex mirror incidence angle α_p. The remaining parameters that define the spectrometer are calculated by applying the formulas in block diagram shown in Fig. 5.

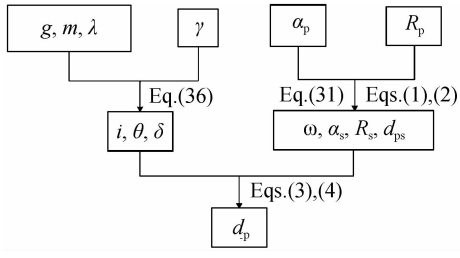

Fig. 5 Block diagram for calculating optical parameters of the spectrometer

5 Case design and analysis

The spectrometer which works in the far-ultraviolet spectral region (120～180 nm) is designed for atmospheric and ionospheric detection. A UV sensitive CCD with a size of 20.5×10.3 mm^2 (pixel size is 20×20 μm^2, and pixel number is 1024×512) and a grating with 1 200 grooves /mm are used. The optical design program ZEMAX was used to perform the ray-tracing and the analysis of aberration. The initial parameters are calculated by using the design

procedure presented above. At last, an optimized system is generated with the help of ZEMAX. The initial and optimized parameters are shown in Table 1. The optimized layout of the spectrometer is shown in Fig. 6.

Table 1 Optical parameters of the spectrometer

Parameters	$\alpha_1=\alpha_4$/(°)	$\alpha_2=\alpha_3$/(°)	$R_1=R_4$/mm	$R_2=R_3$/mm	i/(°)	θ/(°)	γ/(°)	d_{12}/mm	λ_0/nm
Initial	7.746	20	507.51	200	−6.25	16.79	5.27	314.945	150
Optimized	7.746	20	491.72	192.45	−7.37	18.97	5.8	304.76	164
Features	F	F	V	V	V	V	V	V	V

F represents fixed; V represents variable

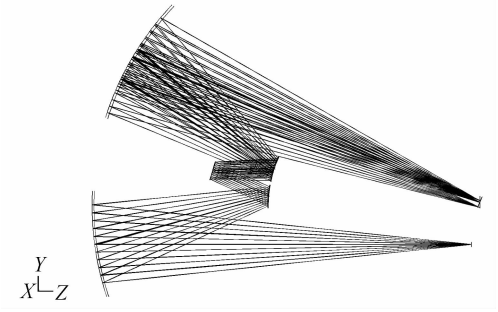

Fig. 6 The optimized layout of the spectrometer based on concentric off-axis dual reflector system

The values of optimized parameters in Table 1 are used to create the final spectrometer, with a slit length of 8 mm, F number of 4.9 and focal length of 82.5 mm. It should be noted that some initial parameters ($\alpha_1=\alpha_4$, $\alpha_2=\alpha_3$) are used directly without further optimization. To first show that astigmatism is eliminated, spot diagram of the on-axis point for the central wavelength at 150 nm is presented in Fig. 7. In fact, it reveals residual oblique spherical aberration. Tangential and sagittal curve for a 8 mm slit and the central wavelength at 150 nm is shown in Fig. 8. The value of astigmatism is zero for the on-axis point and keeps small for the full filed. However, there is a notable field curvature in the full field of view, which should be taken into consideration while using large slit.

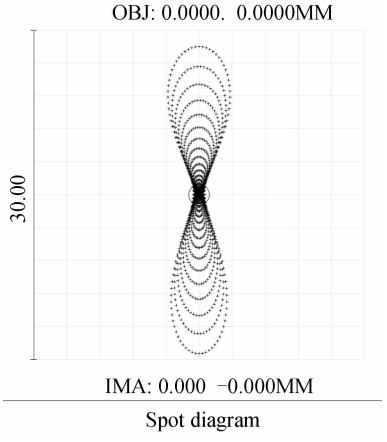

Fig. 7 Spot diagram of the on-axis point for the central wavelength at 150 nm

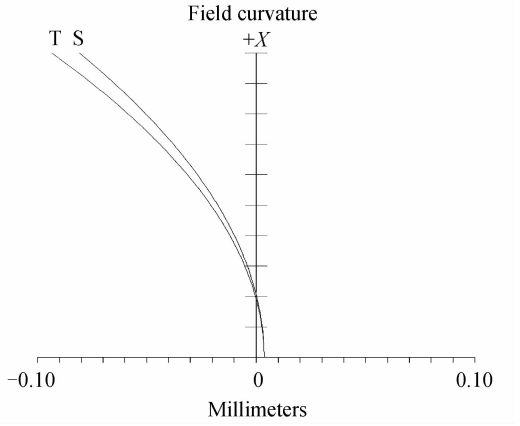

Fig. 8 Tangential and sagittal curve for a 8 mm slit and the central wavelength at 150 nm

To elaborate on the necessity of the relationship between α_1 (α_4) and α_2 (α_3), variations of RMS spot radius with changes of the wavelengths for different configurations are shown in Fig. 9. The comparative spectrometers are created from the same initial structure as the optimized one. In this step, the parameter α_2 (α_3) is set to the variable and automatic optimization tools of the ZEMAX are applied at two different wavelengths (150 nm and 164 nm) to obtain excellent imaging properties. Obviously, as shown in Fig. 9 (a), minimum spot size across the designed wavelength is obtained when the Eq. (29) is met. However, as observed from Fig. 9 (b) and (c), the quality of image in comparative spectrometers is not so good as in optimized spectrometer.

It is also clear that the small spot sizes are only achieved in the vicinity of the central wavelength and short wavelength (see Fig. 9 (a)). Actually, in order to obtain excellent imaging quality over the whole field and spectral range, the central wavelength are adjusted from the initial 150 nm to final 164 nm. By final optimization, the RMS spot radius of the optimized spectrometer is less than 8 μm over the whole working wavelength, and the smaller spot sizes still exist near the central wavelength.

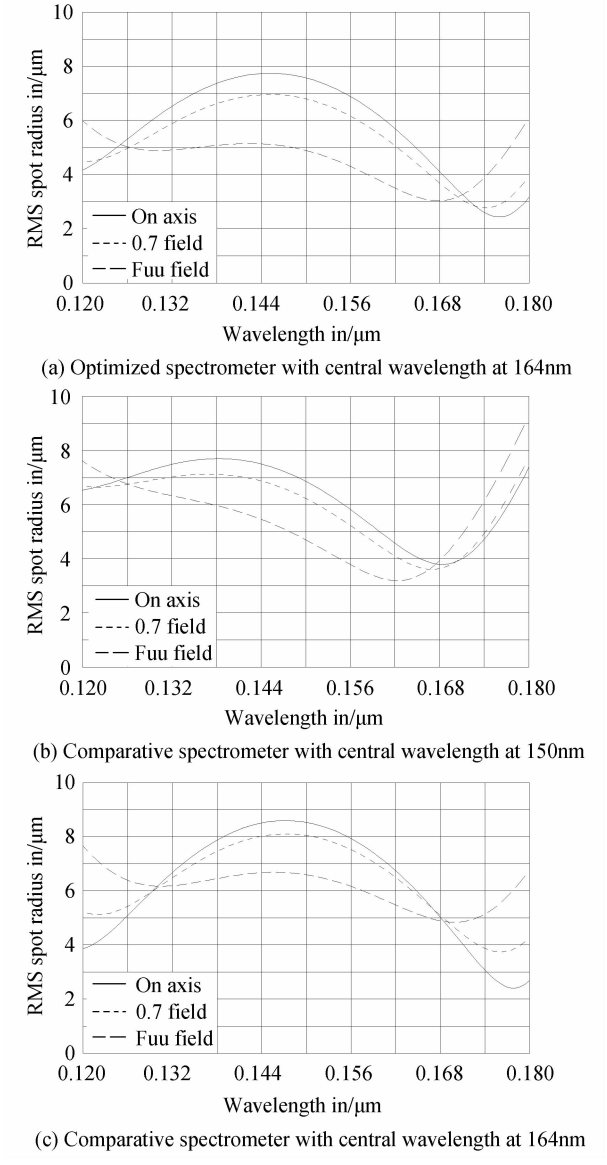

Fig. 9 RMS spot radius versus wavelength for three different fields

Furthermore, another direct confirmation of the astigmatic elimination is found and presented in Table 2. The comparative spectrometers in which Eq. (29) is not met exist larger astigmatism coefficient than that met. The closer the angle $\alpha_2(\alpha_3)$ gets to 20°, the smaller astigmatism coefficient becomes. It means that the configuration satisfying Eq. (29) may be the optimal structure in the search range. At least, it is the local minima in this example.

Table 2 Residual astigmatism in spectrometer

Spectrometer	Central wavelength(λ_0)	$\alpha_1=\alpha_4$ $\alpha_2=\alpha_3$	Astigmatism coefficient W_{222}
Optimized	164 nm	7.746° 20°	$0.995\lambda_0$
Comparative	150 nm	7.746° 19.73°	$1.467\lambda_0$
Comparative	164 nm	7.746° 19.81°	$1.196\lambda_0$

Fig. 10 shows RMS spot radius as a function of slit height for three wavelengths. With regard to the curve for marginal wavelengths, the larger the height of the slit, the bigger the spot size. The bigger geometrical spot size prevents the spectrometer from utilizing large slit unless special care is taken to reduce the spot size for marginal wavelength. However, the dimension of RMS spot radius is less than 10.5 μm and the curve for central wavelength remains under the limit of 5.5 over the whole field. It demonstrates that excellent imaging quality is obtained over the whole field. The modulation transfer function (MTF) of the central and marginal wavelengths in each field is given in Fig. 11 to provide a

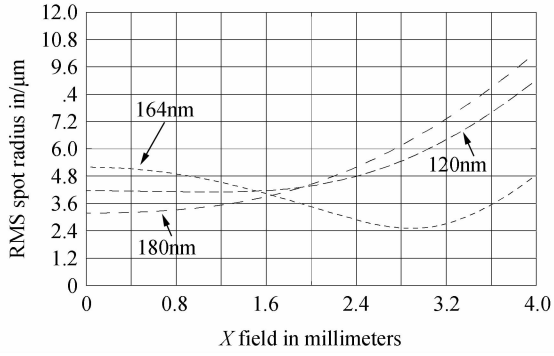

Fig. 10 RMS spot radius versus slit height for three different wavelengths

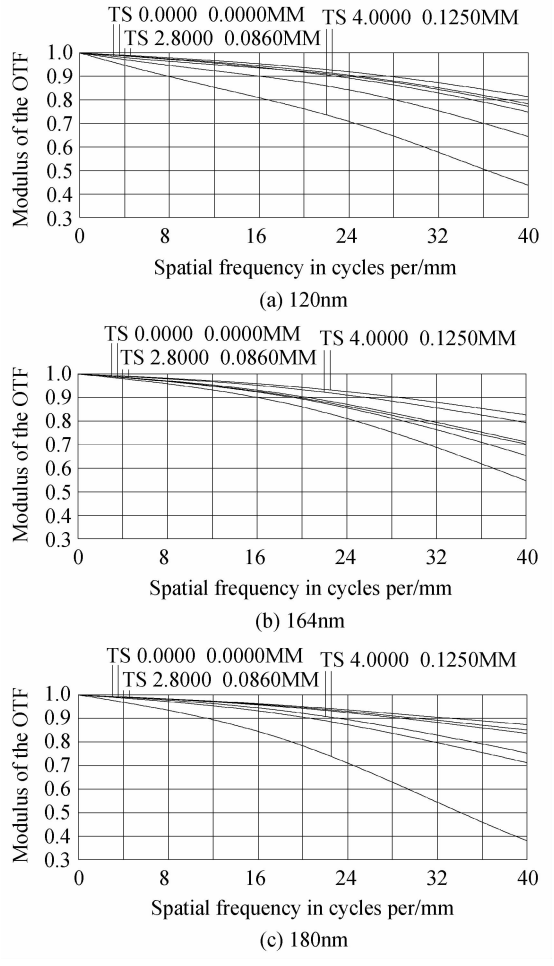

Fig. 11 MTF of the optimized spectrometer at the central and marginal wavelengths

comprehensive characterization of the optimized spectrometer. It is clear that the MTF in each field is larger than 0.37 at 40 lp/mm, and larger than 0.68 at the Nyquist frequency (25 lp/mm), which indicates that the optimized spectrometer will obtain excellent image quality in image plane.

6 Conclusion

The most important aberration in spectrometer configuration is astigmatism which has been reduced or removed by a variety of methods. An anastigmatic spectrometer based on concentric off-axis dual reflector system is proposed in this paper. By using concentric off-axis dual reflector system in both the collimating and the condensing optics, an expression for the astigmatic elimination is derived based on aberration theory and optical path-length concept. Finally, utilizing the presented design procedure, a specific concentric and symmetrical spectrometer with high image quality was designed to show the effectiveness of astigmatic elimination. This is an extension and verification of the author Mouriz′s work.

It should be emphasized here that the coma and spherical aberration are almost zero in the spectrometer based on concentric off-axis dual reflector system. In fact, the concentric off-axis dual reflector system can be obtained by using the off-axis section of the coaxial configuration, which is named concentric Schwarzschild anastigmat. Each of the three aberrations (spherical aberration, coma, astigmatism) has been corrected in this configuration, in which both the mirrors are spheres[16]. However, there is a notable field curvature in concentric Schwarzschild optical system, which should be taken into consideration while using large slit during the spectrometer based on concentric off-axis dual reflector system. It should also be emphasized that elimination of astigmatism is satisfied for the central wavelength. Note that, due to the different diffraction angles at the grating, the incidence angles at the third mirror vary with the wavelength. It means that the stigmatic condition derived in section 3 is not met any longer except for the central wavelength. It shows the way of subsequent research: elimination of the astigmatism over a broad spectral region for the spectrometer based on concentric off-axis dual reflector system.

References

[1] SELLAR R G, BOREMAN G D. Classification of imaging spectrometers for remote sensing applications[J]. *Optical Engineering*, 2005, **44**(1): 013602.

[2] PAXTON L J, CHRISTENSENB A B, MORRISON D, *et al*. GUVI: a Hyperspectral Imager for Geospace[C]. SPIE, 2004, **5660**: 228-240.

[3] READER J. Optimizing Czerny-Turner spectrographs: a comparison between analytic theory and ray tracing[J]. *Journal of the Optical Society of America*, 1969, **59**(9): 1189-1196.

[4] SHAFER A B, MEGILL L R, DROPPLEMAN L. Optimization of the Czerny-Turner spectrometer[J]. *Journal of the Optical Society of America*, 1964, **54**(7): 879-887.

[5] FUTAMATA M, TAKENOUCHI T, KATAKURA K. Highly efficient and aberration-corrected spectrometer for advanced Raman spectroscopy[J]. *Applied Optics*, 2002, **41**(22): 4655-4665.

[6] XU L, CHEN K, HE Q, *et al*. Design of freeform mirrors in Czerny-Turner spectrometers to suppress astigmatism[J]. *Applied Optics*, 2009, **48**(15): 2871-2879.

[7] BATES B, MCDOWELL M, NEWTON A C. Correction of astigmatism in a Czerny-Turner spectrograph using a plane grating in divergent illumination[J]. *Journal of Physics E: Scientific Instruments*, 1970, **3**: 206-210.

[8] DALTON M L. Astigmatism compensation in the Czerny-Turner spectrometer[J]. *Applied Optics*, 1966, **5**(7): 1121-1123.

[9] MCDOWELL M. Design of Czerny-Turner spectrographs using divergent grating illumination[J]. *Optical Acta*, 1975, **22**(5): 473-475.

[10] LEE K S, THOMPSON K P, ROLLAND J P. Broadband astigmatism corrected Czerny-Turner spectrometer[J]. *Optical Express*, 2010, **18**(22): 23378-23384.

[11] ROSENDAHL G R. Contributions to the optics of mirror systems and gratings with oblique incidence. Ⅲ. Some applications[J]. *Journal of the Optical Society of America*, 1962, **52**(4): 412-415.

[12] GOTO M, MORITA S. Spatial distribution measurement of atomic radiation with an astigmatism-corrected Czerny-Turner type spectrometer in the large helical device[J]. *Review of Scientific Instruments*, 2006, **77**: 10F124.

[13] MOURIZ M D, LAGO E L, BLANCO X P, *et al*. Schwarzschild spectrometer[J]. *Applied Optics*, 2011, **50**(16): 2418-2424.

[14] BEUTLER H G. The theory of the concave grating[J]. *Journal of the Optical Society of America*, 1945, **35**(5): 311-350.

[15] CHANG S, PRATA A. Geometrical theory of aberrations near the axis in classical off-axis reflecting telescopes[J]. *Jurnal of the Optical Society of America*, 2005, **22**(11): 2454-2464.

[16] WETHERELL W B, RIMMER M P. General analysis of aplanatic cassegrain, gregorian, and schwarzschild telescopes[J]. *Applied Optics*, 1972, **11**(12): 2817-2832.